Applied Catalysis B: Environmental 100 (2010) 229–237

Contents lists available at ScienceDirect

Applied Catalysis B: Environmental

journal homepage: www.elsevier.com/locate/apcatb

Ultrasound-assisted nanocasting fabrication and excellent catalytic performance of three-dimensionally ordered mesoporous chromia for the combustion of formaldehyde, acetone, and methanol

Yunsheng Xia [a], Hongxing Dai [a,*], Lei Zhang [a], Jiguang Deng [a], Hong He [a], Chak Tong Au [b]

[a] Laboratory of Catalysis Chemistry and Nanoscience, Department of Chemistry and Chemical Engineering, College of Environmental and Energy Engineering, Beijing University of Technology, Beijing 100124, China
[b] Department of Chemistry, Hong Kong Baptist University, Kowloon Tong, Hong Kong, China

ARTICLE INFO

Article history:
Received 24 November 2009
Received in revised form 3 June 2010
Accepted 30 July 2010
Available online 7 August 2010

Keywords:
Mesoporous chromia catalyst
Ultrasound-assisted nanocasting method
KIT-6-templating strategy
Volatile organic compound combustion

ABSTRACT

Rhombohedral chromia with three-dimensionally (3D) ordered mesopore structures were fabricated adopting the ultrasound-assisted nanocasting strategy with 3D ordered mesoporous silica (KIT-6) as hard template and chromium nitrate as metal source. The physicochemical properties of the materials were characterized by the XRD, TGA/DSC, BET, TEM/SAED, XPS, and H_2-TPR techniques, and their catalytic activities were evaluated for the oxidation of typical volatile organic compounds (VOCs), such as formaldehyde, acetone, and methanol. It is found that there were tri-, penta-, and hexavalent chromium ions in the 3D mesoporous structure. Compared to the bulk chromia, the mesoporous chromia materials were larger in surface area (69–124 m^2/g) and could be reduced at lower temperatures. Among the chromia catalysts, the *meso*-Cr-400 one obtained after calcination at 400 °C showed the best performance. Over *meso*-Cr-400 at space velocity = 30,000 mL/(g h), formaldehyde, acetone, and methanol conversions achieved 90% at 117, 124, and 130 °C, respectively; the corresponding apparent activation energies were 45.6, 49.7, and 50.8 kJ/mol. It is concluded that the ultrasound treatment was a key step to improve the mesoporosity quality of the chromia materials during the nanocasting process, and the factors, such as low-temperature reducibility, 3D ordered mesoporous architecture, and high-surface area, were responsible for the excellent catalytic performance of *meso*-Cr-400.

1. Introduction

Volatile organic compounds (VOCs, e.g., aldehydes, ketones, alcohols, esters, aromatics, and aliphatic hydrocarbons) emitted from industrial and transportation activities are major pollutants to the environment. Most of them are malodorous and toxic, and contribute to the formation of photochemical smog [1]. Among the methods for VOCs removal, catalytic combustion is generally accepted to be the most effective since it guarantees the complete oxidation of VOCs to CO_2 and H_2O [2].

In the past decades, a large number of catalysts, including metal oxides (MO_x, M = Co, Mn, Cu or Cr [3–5]) and perovskite-type oxides ($La_{1-x}Sr_xMO_3$, M = Mn or Co [6,7]), have been investigated for the removal of VOCs. Compared to the precious metal-based catalysts, the ones based on other metals are inferior in low-temperature activity but cheaper in cost. For example, a 100% conversion of formaldehyde to CO_2 and H_2O was reported over Fe^{3+}-doped 5A molecular sieves in the 160–190 °C range at a space velocity (SV) of 50,000 h^{-1} [8]. Tang et al. [9] observed 100% formaldehyde conversion over manganese oxide nanorods under the conditions of formaldehyde concentration = 0.01 vol%, SV = 24,000 h^{-1}, and temperature = 180 °C. After studying the catalytic activities of three kinds of tunnel-structured manganese oxides, Hao and co-workers [10] reported that the crystomelane catalyst performed the best, giving a 100% HCHO conversion at 140 °C and 18,000 h^{-1}. Furthermore, complete combustion of a mixture of formaldehyde and methanol over 18.2 wt% Mn/Al_2O_3 at 220 °C was observed by Álvarez-Galván et al. [11]. After investigating the oxidation of acetone with excess oxygen over Mn_3O_4, Baldi et al. [12] pointed out that acetone was partially oxidized to acetaldehyde and acetic acid at ca. 200 °C, but completely converted to CO_2 and H_2O at 270 °C. Working on the catalysis of silica- and alumina-supported manganese oxides for acetone oxidation in the presence of ozone, Oyama and co-workers [13] observed that the 10 wt% MnO_x/Al_2O_3 catalyst outperformed the 10 wt% MnO_x/SiO_2 catalyst, and acetone could be completely oxidized to CO_2 and H_2O below 300 °C at 15,000 h^{-1}.

* Corresponding author. Tel.: +86 10 6739 6588; fax: +86 10 6739 1983.
E-mail address: hxdai@bjut.edu.cn (H. Dai).

0926-3373/$ – see front matter © 2010 Elsevier B.V. All rights reserved.
doi:10.1016/j.apcatb.2010.07.037

It is believed that catalytic activities are associated with the surface area, oxygen defect, and transition-metal ion redox ability (reducibility) of the catalyst. A good approach for increasing surface area of a material is to have it fabricated in the form of mesoporous structure. Recently, well-ordered mesoporous oxides of Mn [14], Cr [15], Fe [16], and Co [17] were generated using the surfactant-templating methods or adopting the nanocasting routes with solid porous materials (e.g., three-dimensionally (3D) ordered mesoporous silica (KIT-6) and 3D ordered mesoporous carbon) as hard template [18]. For example, using poly(alkylene oxide) as surfactant, KIT-6 as template, and chromium nitrate as precursor, Sinha and Suzuki [19,20] obtained high-surface-area (78 m^2/g) 3D mesoporous chromia after calcining the as-obtained material at 500 °C, and found that the mesoporous material displayed excellent catalytic performance in toluene combustion. The authors ascribed the unusual performance to the presence of multivalent Cr ions.

In the past several years, we have reported the fabrication of a number of nano- and porous materials employing the hydrothermal methods, and observed good catalytic activities of $LaCoO_3$/SBA-15 [21] and $La_{1-x}Sr_xMO_3$ (M = Co, Mn; x = 0–0.6) [22–27] in the combustion of toluene and/or ethyl acetate. Recently, we have successfully synthesized a series of 3D ordered mesoporous chromia in an autoclave via a solvent-free route using KIT-6 as hard template, and found that the materials exhibited exceptionally high performance in catalyzing the oxidation of toluene and ethyl acetate [28]. In this paper, we report the ultrasound-assisted nanocasting strategy for the fabrication of 3D ordered mesoporous chromia by using KIT-6 as template and chromium nitrate as Cr source. The fabrication, characterization, and catalytic activities of the 3D ordered mesoporous chromia materials were investigated for the combustion of formaldehyde, acetone, and methanol.

2. Experimental

2.1. Catalyst preparation

Mesoporous silica (KIT-6) was synthesized by adopting the procedure described by other researchers [29]. In a typical procedure, 6.0 g of poly(ethylene glycol)–block–poly(propylene glycol)–block–poly(ethylene glycol) ($EO_{20}PO_{70}EO_{20}$, Pluronic P123, $MW_{aver.}$ = 5800, Aldrich) was dissolved in a mixture of 217.0 g of deionized water and 11.8 g of HCl solution (35 wt%). Then, 6.0 g of *n*-butanol (Beijing Chemical Reagents, 99.4%) was added to the mixture at 35 °C under stirring. After the mixture was further stirred for 1 h, 12.9 g of tetraethyl orthosilicate (TEOS, Beijing Chemical Reagents, 98%) was added. The molar ratio of TEOS:P123:HCl:H_2O:*n*-butanol was 1:0.017:1.83:195:1.31. The as-resulted mixture was continuously stirred at 35 °C for 24 h, then transferred to a 100-mL Teflon-lined stainless steel autoclave (packed volume = ca. 75 mL) and finally placed in an oven for hydrothermal treatment at 100 °C for 24 h. After being in turn filtered, washed 3 times with deionized water and absolute ethanol, dried at 60 °C for 12 h, and ground, the obtained white powders were heated in air at a ramp of 1 °C/min from room temperature (RT) to 550 °C and kept at 550 °C for 4 h, thus generating the KIT-6 material.

The mesoporous chromia catalysts were fabricated adopting the ultrasound-assisted impregnation strategy. In a typical fabrication, 1.0 g of $Cr(NO_3)_3{\cdot}9H_2O$ (Beijing Chemical Reagents, 99.5%) was dissolved in 10 mL of ethanol, and then 0.5 g of KIT-6 was added to the Cr-containing ethanol solution. After ultrasound-assisted dispersion at 40 °C for 100 min, the mixture was heated in a nitrogen flow (30 mL/min) at a ramp of 1 °C/min from 40 °C to 200, 300, 400 or 500 °C and maintained at this temperature for 4 h. The resulting powders were treated twice with a 10% HF aqueous solution (for the complete removal of the KIT-6 template), washed 3–4 times with deionized water and then dried at 60 °C for 24 h. The mesoporous chromia samples calcined at 200, 300, 400 and 500 °C are denoted as *meso*-Cr-200, *meso*-Cr-300, *meso*-Cr-400, and *meso*-Cr-500, respectively, hereinafter. For comparison purposes, the chromia catalyst (denoted as *meso*-Cr′-400) was fabricated and calcined at 400 °C for 4 h according to the above method in the absence of ultrasound irradiation; a bulk chromia catalyst (denoted as *bulk*-Cr) was also prepared by direct decomposition of nitrate chromium in air at 500 °C. It should be noted that chromium is a sensitive element to the environment and HF acid is also harmful. Therefore, appropriate post-treatments of the chromia catalysts and HF acid after use should be made to avoid any pollution to the environment.

2.2. Catalyst characterization

Small- and wide-angle X-ray diffraction (XRD) patterns of the samples were collected on a Bruker/AXS D8 Advance instrument operated at 40 kV and 40 mA using Cu Kα irradiation and nickel filter (λ = 0.15406 nm). High-resolution transmission electron microscopic (HRTEM) images as well as the selected-area electron diffraction (SAED) patterns of the samples were acquired on a JEOL JEM-2010 apparatus. Thermogravimetric analysis (TGA) and differential scanning calorimetric (DSC) experiments were performed on a Pyris Diamond thermal analyzer, having the sample heated in air (20 mL/min) from RT to 600 °C at a rate of 10 °C/min. Surface areas and pore size distributions as well as N_2 adsorption–desorption isotherms of the samples were measured by means of N_2 adsorption at −196 °C using a Micromeritics ASAP 2020 apparatus, with the sample being first degassed at 200 °C for 3 h; the surface area and pore size distribution were calculated according to the Brunauer–Emmett–Teller (BET) and Barrett–Joyner–Halenda (BJH) methods, respectively. The X-ray photoelectron spectroscopic (XPS) technique was used to determine the O 1s and Cr 2p binding energies (BEs) of surface oxygen and chromium species, using Mg Kα ($h\nu$ = 1253.6 eV) as excitation source. Before XPS measurement, the sample was treated in an O_2 flow of 20 mL/min at 200 °C for 1 h. After cooling to RT, the sample was transferred to a holder in a Glove Bag (Instruments for Research and Industry, USA) that was filled with helium. After being transferred into the spectrometer chamber, the sample was degassed in the preparation chamber for 0.5 h before being analyzed in the analysis chamber. The BE values of O 1s and Cr 2p were calibrated against the C 1s signal (BE = 284.6 eV) of contaminant carbon.

Hydrogen temperature-programmed reduction (H_2-TPR) experiments were carried out in the RT–650 °C range on an AutoChem II 2920 (Micromeritics) apparatus. The sample was pretreated in an O_2 flow of 25 mL/min at 200 °C for 1 h and then cooled down to RT in the same atmosphere. The sample was finally reduced in a 5% H_2–95% Ar flow of 30 mL/min at a ramp of 15 °C/min. The outlet gases were analyzed on-line using a thermal conductivity detector (TCD). The TCD responses were calibrated against that of the complete reduction of a standard powdered CuO sample (Aldrich, 99.995%).

2.3. Catalytic evaluation

The catalytic activity was evaluated with the sample charged in a continuous flow fixed-bed quartz micro-reactor (i.d. = 4 mm). 0.1 g of the catalyst (40–60 mesh) was diluted with an equal volume of quartz sands (40–60 mesh) to avoid temperature gradients. The reactant was fed to the reactor by a flow of N_2 that passed through a container filled with an aqueous solution of 37% formaldehyde, acetone or methanol. The temperature of the aqueous formaldehyde, acetone or methanol solution was kept at 0 °C by having the container immersed in an ice/water bath. The reactant feed (flow rate,

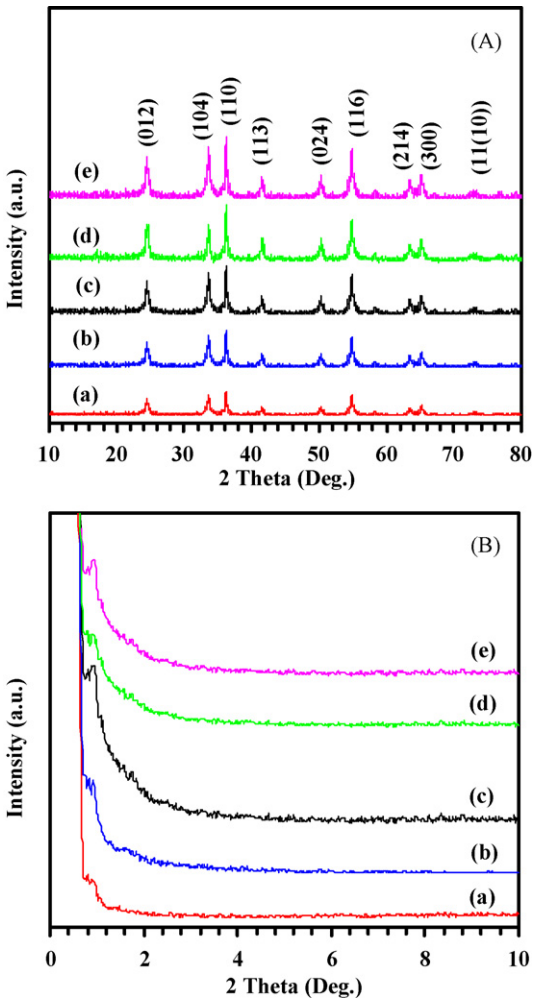

Fig. 1. (A) Wide-angle and (B) small-angle XRD patterns of (a) *meso*-Cr-200, (b) *meso*-Cr-300, (c) *meso*-Cr-400, (d) *meso*-Cr′-400, and (e) *meso*-Cr-500.

50 mL/min) was 500 ppm VOC + O_2 + N_2 (balance) with a VOC/O_2 molar ratio of 1/300 and SV of 30,000 mL/(g h). To change the SV, we altered the amount of catalyst. Prior to reaction, the catalyst was treated with the reactant mixture at 80 °C for 1.5 h to avoid over estimation (caused by adsorption) of formaldehyde, acetone or methanol conversion. The product analysis was conducted after 20 min of on-stream reaction at a selected temperature. The outlet mixture was analyzed on-line by a gas chromatograph (Shimadzu GC-2010) equipped with a TCD, using a Chromosorb 101 column for formaldehyde, acetone or methanol and a Carboxen 1000 column for permanent gas separation. The balance of carbon throughout the study was estimated to be around 99.5%.

3. Results and discussion

3.1. Crystal structure

Fig. 1 shows the small- and wide-angle XRD patterns of the chromia catalysts. It can be seen from Fig. 1A that the crystallinity of chromia catalysts improved with the rise of calcination temperature. By referring to the XRD pattern (JCPDS No. 84-1616) of standard Cr_2O_3, one can realize that the structure of the four catalysts was rhombohedral, and the peaks were indexed as shown in Fig. 1A(e). There was the detection of a signal at 2θ = ca. 0.9° (Fig. 1B), indicating the formation of mesoporous structure. When the calcination temperature is above 300 °C, the intensity of the 2θ = ca. 0.9° signal increases markedly (Fig. 1B(c and e)), suggesting the improvement in mesoporosity. It should be noted that the *meso*-Cr′-400 sample prepared without ultrasound showed a weaker signal at 2θ = ca. 0.9°, meaning that the meoporous structure of this sample was poorer than that of the counterpart derived with ultrasound. In other words, the utilization of ultrasonic irradiation during the fabrication process facilitated the melioration in mesopore structure of the chromia sample.

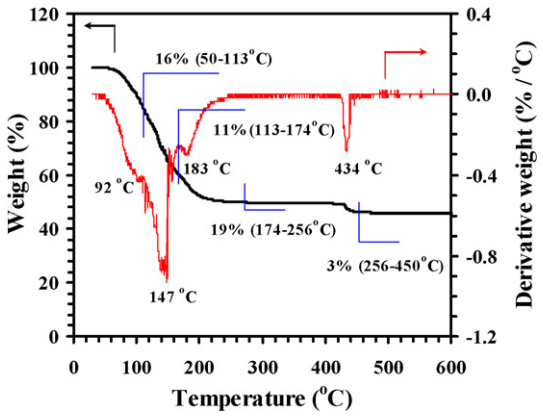

Fig. 2. TGA/DSC profiles of the chromium nitrate-impregnated KIT-6 sample.

Fig. 2 depicts the TGA and DSC profiles of the KIT-6 sample that was impregnated with chromium nitrate. Four signals of weight losses were observed in the 50–113, 113–174, 174–256, and 256–450 °C regions, corresponding to weight losses of 16, 11, 19, and 3 wt%. The first two were due to the removal of water in chromium nitrate crystals [30,31], the third one was attributed to the decomposition of $Cr(NO_3)_3$ (giving Cr_2O_3), and the last one to the partial removal of oxygen from the Cr_2O_3 lattice [30,31]. From Fig. 2, one can notice that above 200 °C, there was almost no weight loss, except the weight loss due to lattice oxygen removal at 434 °C. The result indicates that it is appropriate to calcine the chromium nitrate-impregnated KIT-6 sample in the 200–500 °C range.

3.2. Pore structure and surface area

Nitrogen adsorption–desorption isotherms and the pore size distributions of the *meso*-Cr-200, *meso*-Cr-300, *meso*-Cr-400, and *meso*-Cr-500 catalysts are shown in Fig. 3, and the related surface areas and pore parameters are summarized in Table 1. From Fig. 3A, one can observe a big hysteresis loop in the relative pressure range of 0.5–1.0 over the five catalysts, indicating the presence of mesopores [32,33]. Furthermore, an additional small hysteresis loop was detected over *meso*-Cr-300 in the p/p_0 = 0.4–0.6 range, and two additional small hysteresis loops were observed over *meso*-Cr-400 and *meso*-Cr-500 in the p/p_0 = 0.3–0.6 and p/p_0 = 0.4–0.7 range, respectively. Similar sorption isotherms of mesoporous chromia were reported by Wang et al. [34]. From Table 1, one can see that the surface area of the *bulk*-Cr sample (nonporous) was 5 m^2/g.

Table 1
Textural properties of KIT-6 and the chromia catalysts.

Sample	Surface area (m^2/g)	Average pore diameter (nm)	Pore volume (cm^3/g)
KIT-6	790	6.1	0.95
bulk-Cr	5	–	–
meso-Cr-200	91	7.7	0.13
meso-Cr-300	98	7.6	0.14
meso-Cr-400	124	7.9	0.21
meso-Cr′-400	69	8.2	0.12
meso-Cr-500	109	8.9	0.16

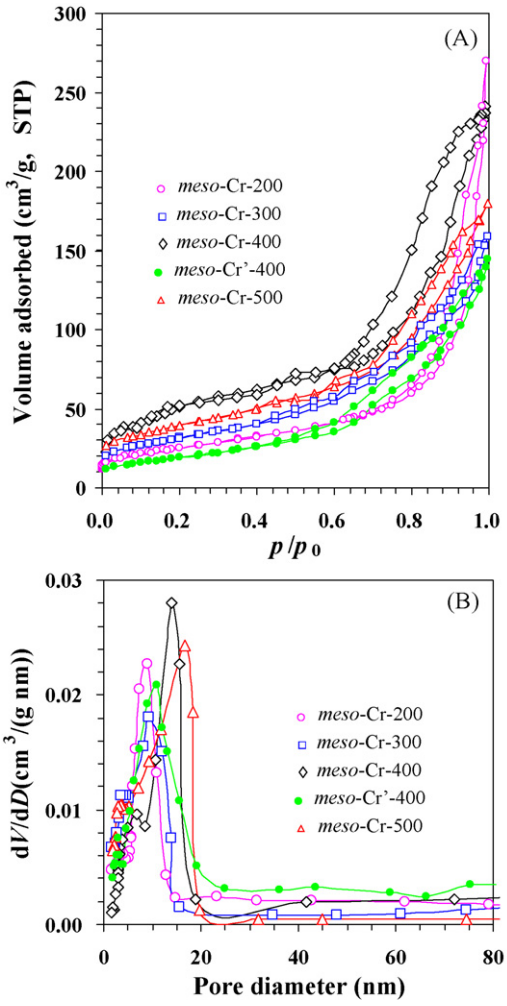

Fig. 3. (A) Nitrogen adsorption–desorption isotherms and (B) pore size distributions of the chromia catalysts.

Despite lower than KIT-6 (790 m^2/g) in surface area, the mesoporous chromia were much higher than *bulk*-Cr in surface area. With the rise of calcination temperature from 200 to 500 °C, the surface area of the mesoporous chromia first increased and then decreased, and the *meso*-Cr-400 catalyst was the highest in surface area (124 m^2/g). Compared to *meso*-Cr-400, *meso*-Cr-500 (109 m^2/g) was lower in surface area, plausibly a result of the partial collapse of mesopores at 500 °C. Nonetheless, the surface areas of *meso*-Cr-200, *meso*-Cr-300, *meso*-Cr-400, and *meso*-Cr-500 catalysts were higher than those (82–86 m^2/g) of mesoporous chromia reported by Wang et al. [34] and Jiao et al. [35]. However, the surface area of the ultrasound-free derived *meso*-Cr′-400 sample was much lower than that of the ultrasound-assisted derived *meso*-Cr-400 sample. Fig. 3B shows the pore size distributions of the five catalysts. There were two peaks at 3.7 and 9.1 nm, 3.6 and 9.4 nm, 6.7 and 13.9 nm, 3.0 and 11.1 nm, and 3.1 and 16.8 nm observed over *meso*-Cr-200, *meso*-Cr-300, *meso*-Cr-400, *meso*-Cr′-400, and *meso*-Cr-500, respectively. Compared to KIT-6, the five catalysts were larger in average pore size but significantly lower in pore volume (Table 1).

Theoretically speaking, via a hard template nanocasting route, the pore diameter and wall thickness of the final product are equal to the wall thickness and pore diameter of the hard template, respectively [18,36]. Actually, however, it is not true in most cases. The reason is that there is a difference in physicochemical property of the final product and the hard template. Due to the discrepancy in physicochemical property of Cr_2O_3 and SiO_2 (KIT-6), we did not obtain mesoporous chromia materials that possessed the pore diameter and wall thickness same as the corresponding wall thickness and pore diameter of KIT-6. Furthermore, the failure in perfect replication of the KIT-6 silica by Cr_2O_3 might also be due to the mass transfer along different directions and disconnection of Cr_2O_3 crystals during thermal decomposition and crystallization. Similar results have also been reported by other investigators [35]. Therefore, slight deviations in pore size and pore wall thickness would be inevitable in nanocasting processes [17,37]. However, the utilization of ultrasound irradiation during the KIT-templating nanocasting processes could maximize the infiltration of the Cr precursor solution into mesopores of the KIT-6, thus enhancing the mesoporosity quality of the chromia product.

The TEM images as well as the SAED pattern of the hard template KIT-6 and the four catalysts are shown in Fig. 4. Clearly, KIT-6 showed arrays of well-ordered mesopores. From Fig. 4(b–d, g and h), one can see ordered mesopores of *meso*-Cr-200, *meso*-Cr-300, *meso*-Cr-400, and *meso*-Cr-500, with those of *meso*-Cr-400 displaying the best quality (Fig. 4(d and e)). Similar mesoporous structures were observed by Dickinson et al. [15] and Jiao et al. [36] over the chromia samples derived using KIT-6 as hard template. Compared to *meso*-Cr-400, *meso*-Cr-500 showed clear deterioration in mesoporous structure, possibly due to sintering of chromia at 500 °C as reflected in a drop of surface area (Table 1). The appearance of multiple electron diffraction rings (inset of Fig. 4f) indicates the presence of polycrystalline chromia in *meso*-Cr-400. The lattice spacing of the (1 1 0) plane of *meso*-Cr-400 was estimated to be ca. 0.248 nm, very close to that (0.24758 nm) of Cr_2O_3 (JCPDS No. 84-1616). Similar SAED patterns were recorded over the *meso*-Cr-200, *meso*-Cr-300, and *meso*-Cr-500 samples. The results indicate that all of the four mesoporous chromia possessed polycrystalline mesoporous walls.

3.3. Surface chromium and oxygen species

Fig. 5 shows the Cr $2p_{3/2}$ and O 1s XPS spectra of the *bulk*-Cr and *meso*-Cr-400 catalysts. There was only one asymmetrical Cr $2p_{3/2}$ peak for each of the two catalysts. The Cr $2p_{3/2}$ peak of *meso*-Cr-400 could be deconvoluted to the three components at BE = 576.8, 578.5, and 579.7 eV, whereas that of *bulk*-Cr to the two components at BE = 576.7 and 579.4 eV. The components at BE = 576.7–576.8, 578.5, and 579.4–579.7 eV could be assigned to Cr^{3+}, Cr^{5+}, and Cr^{6+}, respectively [38,39]. The co-presence of Cr^{2+}, Cr^{3+}, Cr^{4+}, Cr^{5+}, and Cr^{6+} species on mesoporous chromia has been reported by Sinha and Suzuki [20]. The results of quantitative analyses on the Cr $2p_{3/2}$ and O 1s spectra are summarized in Table 2. Apparently, the surface Cr^{6+} content on *bulk*-Cr was higher than that on *meso*-Cr-400; in addition, there was a surface Cr^{5+} content of 12.2 mol% on the *meso*-Cr-400 catalyst.

From Fig. 5B, one can see asymmetrical O 1s signals that could be resolved into the two components at BE = ca. 530.6 and 532.7 eV, ascribable to surface lattice oxygen (O_{latt}) and adsorbed oxygen (O_{ads}) species [40,41], respectively. It has been reported that the BE values of lattice oxygen in Cr_2O_3 [42,43] and CrO_3 [42] were 530.0 and 530.5 eV, respectively. The BE value of lattice oxygen in Cr_2O_5 should be in the range of 530.0–530.5 eV. Due to the resolution (0.5 eV) of the XPS analysis, one cannot differentiate the lattice oxygens in Cr_2O_3, Cr_2O_5, and CrO_3 from their O 1s XPS signals. Furthermore, no crystalline phases of Cr_2O_5 and CrO_3 were detected in our chromia samples. Therefore, the co-existence of Cr^{3+}, Cr^{5+}, and Cr^{6+} species would not mean the co-presence of Cr_2O_3, Cr_2O_5, and CrO_3 phases. In other words, the chromia catalysts existed mainly in the form of Cr_2O_3 phase, in which some Cr^{5+} and Cr^{6+} species were generated. The O_{ads}/O_{latt} molar ratio of *meso*-Cr-400 was much higher than that of *bulk*-Cr (Table 2), implying that one

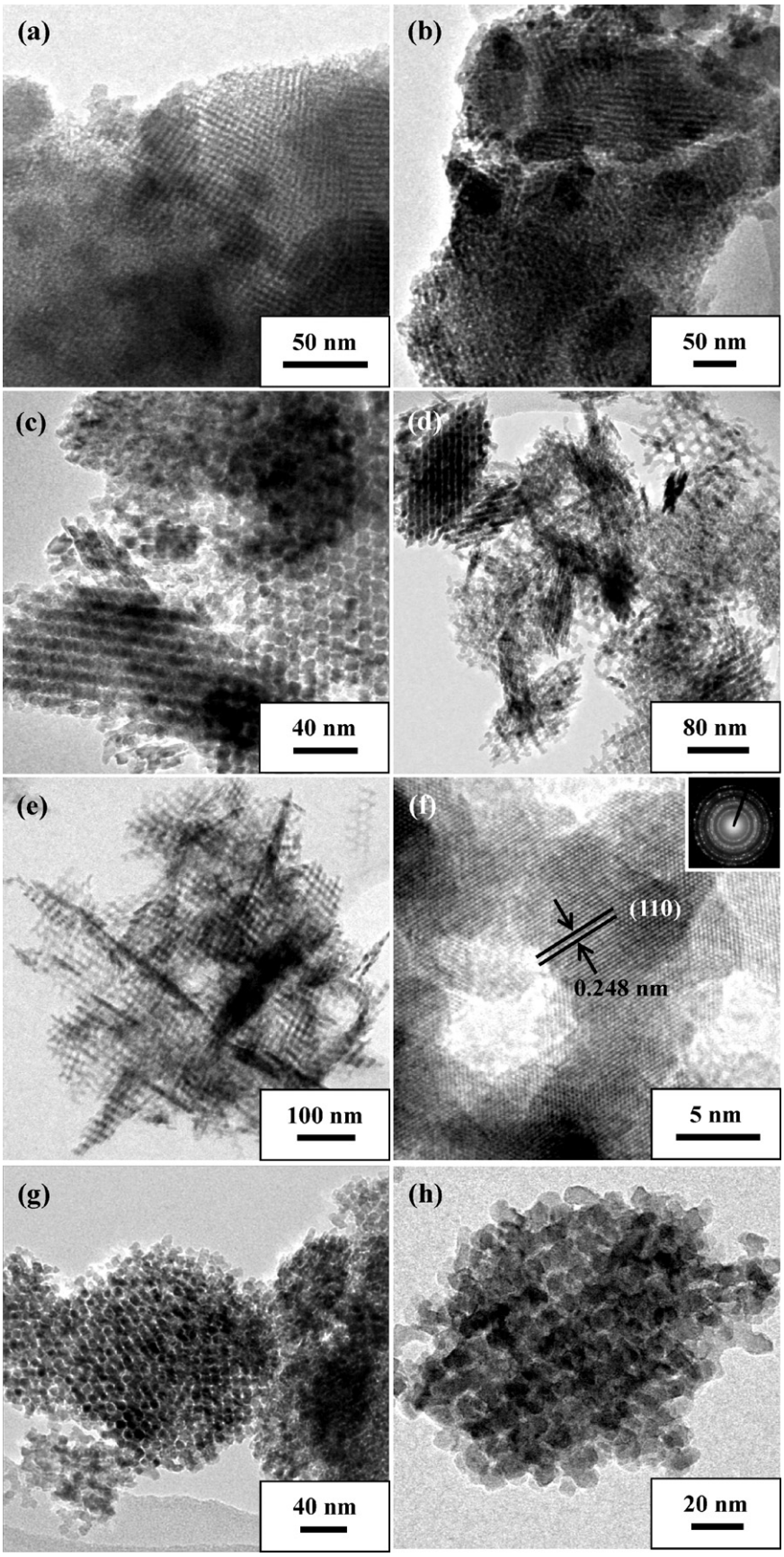

Fig. 4. TEM images and the SAED pattern (inset) of (a) KIT-6, (b) *meso*-Cr-200, (c) *meso*-Cr-300, (d–f) *meso*-Cr-400, and (g and h) *meso*-Cr-500.

Table 2
Surface chromium and oxygen compositions of the *bulk*-Cr and *meso*-Cr-400 catalysts.

Sample	Chromium			Oxygen		
	Cr^{3+} (mol%)	Cr^{5+} (mol%)	Cr^{6+} (mol%)	O_{ads} (mol%)	O_{latt} (mol%)	O_{ads}/O_{latt} (mol/mol)
bulk-Cr	86.9	0	13.1	91.1	8.9	0.10
meso-Cr-400	76.4	12.2	11.4	70.5	29.5	0.42

can enrich the surface of chromia with adsorbed oxygen by creating a mesoporous structure.

3.4. Reducibility

There is discrepancy in the reduction behavior of chromia prepared by adopting different methods and supports [44–46]. The chromia/aluminum pillared bentonite catalyst prepared by Storaro et al. exhibited two reduction bands centered at 391 and 546 °C, attributable to the conversion of Cr^{6+} to Cr^{3+} and Cr^{3+} to Cr^{2+}, respectively [45]. In the reduction of Cr_2O_3 obtained through slow precipitation from a solution of chromium nitrate (induced by ammonia addition) followed by calcination at 600 °C for 6 h, three reduction bands at 190, 350, and 450 °C were observed, the bands at 190 and 350 °C could be ascribed to the reduction of Cr^{6+} to Cr^{3+}, and the one at 450 °C to the reduction of Cr^{3+} to Cr^{2+} [46]. Fig. 6 shows the H_2-TPR profiles and the corresponding initial hydrogen consumption rates of the chromia catalysts. For *bulk*-Cr, there was only one reduction band at 518 °C, corresponding to a H_2 consumption of 7.61 mmol/g. For *meso*-Cr-200, there were two reduction bands, one at 320 and the other at 471 °C, corresponding to H_2 consumption of 1.63 and 6.21 mmol/g, respectively. As for *meso*-Cr-300, *meso*-Cr-400, *meso*-Cr′-400, and *meso*-Cr-500, there were three reduction bands centered at 207–214, 322–354, and 454–464 °C, corresponding to H_2 consumption of 0.59, 1.38, and 6.95 mmol/g for *meso*-Cr-300, 0.66, 2.28, and 6.84 mmol/g for *meso*-Cr-400, 0.37, 1.55, and 5.87 mmol/g for *meso*-Cr′-400, and 0.45, 1.94, and 5.78 mmol/g for *meso*-Cr-500. According to the results reported in the literature [44,45], it is reasonable to assign the reduction bands below 250 °C and in the ranges of 300–400 and 400–550 °C to the reduction of Cr^{5+} to Cr^{3+}, Cr^{6+} to Cr^{3+}, and Cr^{3+} to Cr^{2+}, respectively. In the extreme cases when (i) all of the Cr ions were hexavalent and reduced to Cr^{2+}, the H_2 consumption would be 20.0 mmol/g; and (ii) all of the Cr ions were trivalent and reduced to Cr^{2+}, the H_2 consumption would be 6.58 mmol/g. It is observed that the H_2 consumptions of the chromia catalysts as well as that of the *bulk*-Cr catalyst were in the range of 7.61–9.78 mmol/g. The

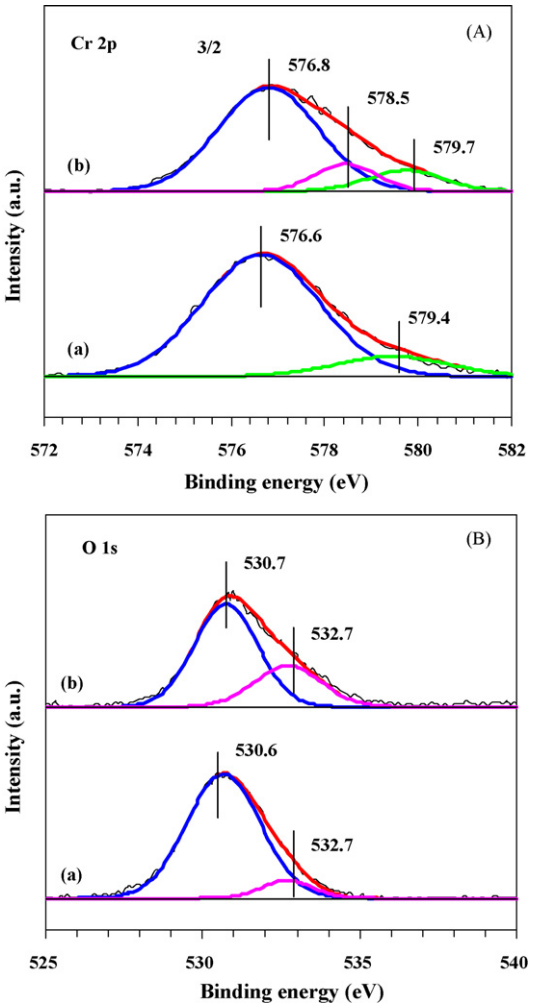

Fig. 5. (A) Cr $2p_{3/2}$ and (B) O 1s XPS spectra of (a) *bulk*-Cr and (b) *meso*-Cr-400.

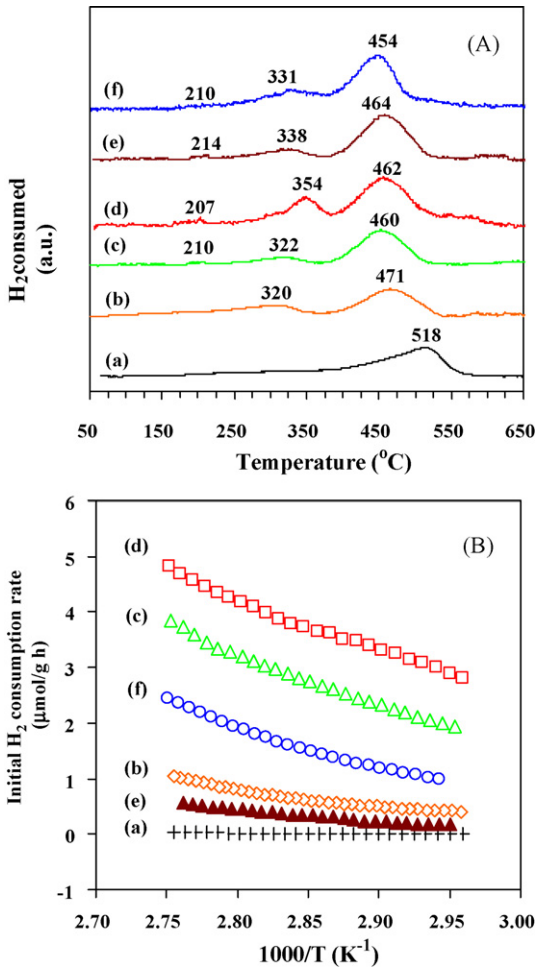

Fig. 6. (A) TPR profiles and (B) initial hydrogen consumption rate as a function of inverse temperature: (a) *bulk*-Cr, (b) *meso*-Cr-200, (c) *meso*-Cr-300, (d) *meso*-Cr-400, (e) *meso*-Cr′-400, and (f) *meso*-Cr-500.

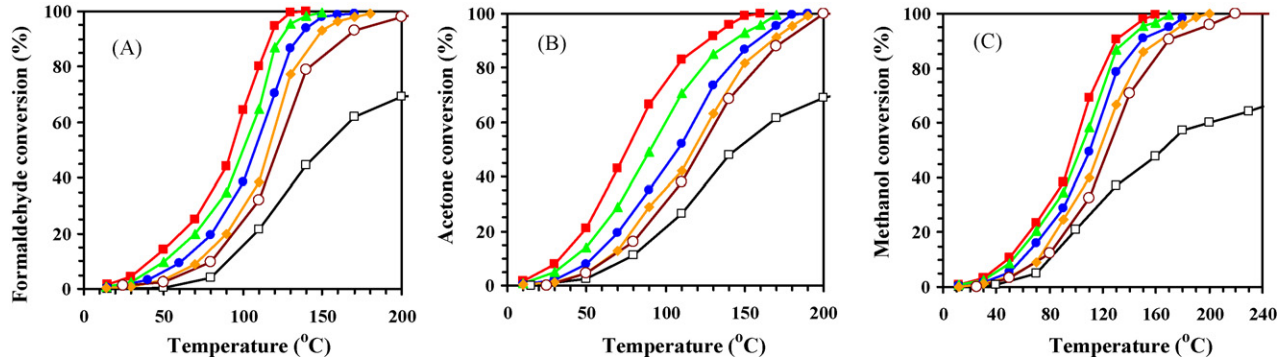

Fig. 7. Catalytic activity versus reaction temperature over *bulk*-Cr (□), *meso*-Cr-200 (♦), *meso*-Cr-300 (▲), *meso*-Cr-400 (■), *meso*-Cr′-400 (○), and *meso*-Cr-500 (●) for the oxidation of (A) formaldehyde, (B) acetone, and (C) methanol under the conditions of VOC concentration = 500 ppm, VOC/O_2 molar ratio = 1/300, and SV = 30,000 mL/(g h).

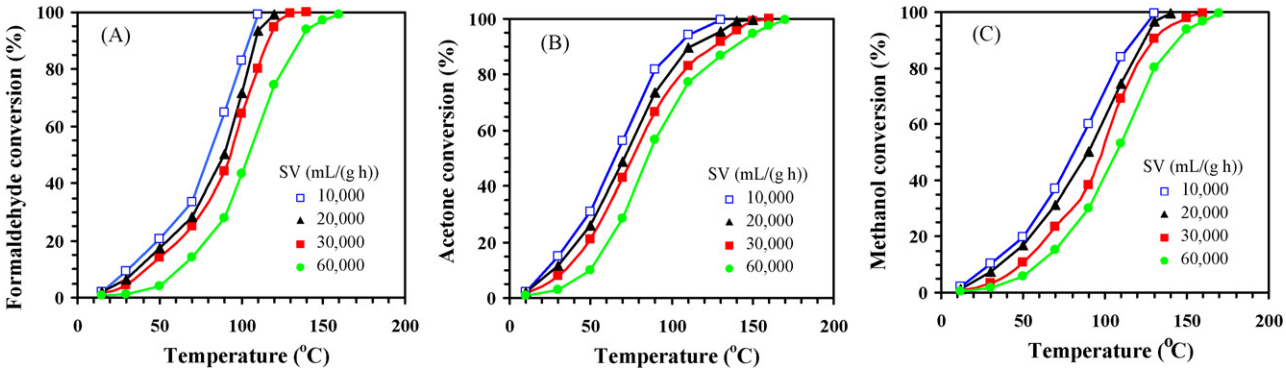

Fig. 8. Effect of SV on the catalytic activity of *meso*-Cr-400 for the oxidation of (A) formaldehyde, (B) acetone, and (C) methanol.

results indicate that there was the co-presence of Cr^{3+}, Cr^{5+}, and Cr^{6+} in the chromia catalysts, in good agreement with the results of XPS investigations.

We use the initial H_2 consumption rate (where reduction was less than 20%) to evaluate the reducibility of the catalysts. As shown in Fig. 6B, the *meso*-Cr-400 catalyst displayed an initial H_2 consumption rate much higher than those of the other catalysts. The initial H_2 consumption rates across the catalysts followed the order of *meso*-Cr-400 > *meso*-Cr-300 > *meso*-Cr-500 > *meso*-Cr-200 > *meso*-Cr′-400 > *bulk*-Cr.

3.5. Catalytic performance

The complete oxidation of formaldehyde, acetone, and methanol were used to test the catalytic activities of the chromia catalysts. In blank runs with only quartz sand particles loaded in the micro-reactor, we detected no oxidation of formaldehyde, acetone, and methanol under the adopted reaction conditions. Fig. 7 shows the catalytic activities of *bulk*-Cr, *meso*-Cr-200, *meso*-Cr-300, *meso*-Cr-400, *meso*-Cr′-400, and *meso*-Cr-500 for the combustion of formaldehyde, acetone, and methanol, and the $T_{10\%}$, $T_{50\%}$, and $T_{90\%}$ data are summarized in Table 3. It is observed that with the rise of reaction temperature, conversion of formaldehyde, acetone or methanol increased over the catalysts, with the mesoporous chromia catalysts significantly outperforming the *bulk*-Cr catalyst. Among the catalysts, *meso*-Cr-400 performed the best, showing 90% conversion of formaldehyde, acetone, and methanol at 117, 124, and 130 °C (Table 3 and Fig. 7), respectively. The catalytic activity decreased in the sequence of *meso*-Cr-400 > *meso*-Cr-300 > *meso*-Cr-500 > *meso*-Cr-200 > *meso*-Cr′-400 > *bulk*-Cr, coinciding with the order of reducibility of the catalysts. The catalytic activities of *meso*-Cr′-400 much lower than those of *meso*-Cr-400 for the addressed reactions demonstrate the promotional effect of ultrasound treatment during the nanocasting process on the enhancement in catalytic performance of the chromia material.

Fig. 8 shows the effect of SV on the catalytic performance of *meso*-Cr-400 for formaldehyde, acetone, and methanol oxidation. As expected, conversion of formaldehyde, acetone or methanol dropped with a rise of SV from 10,000 to 60,000 mL/(g h). Shown in Fig. 9 is the performance of *meso*-Cr-400 within 40 h of on-stream reaction. Apparently, the performance was stable, meaning that the *meso*-Cr-400 material was durable. It is worth pointing out that

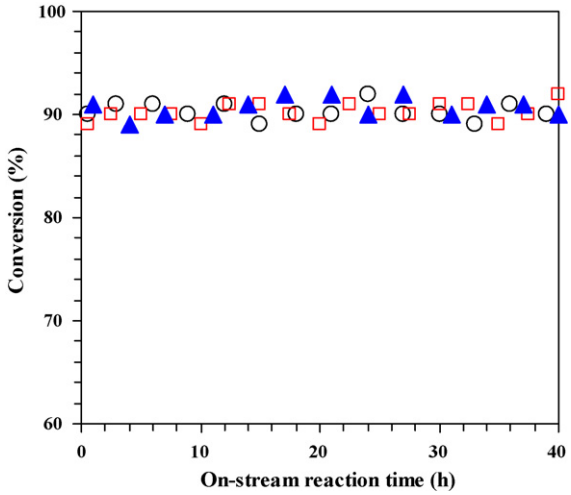

Fig. 9. Catalytic activity versus on-stream reaction time over the *meso*-Cr-400 catalyst for the oxidation of formaldehyde (○), acetone (□), and methanol (▲) at 117, 124, and 130 °C, respectively, under the conditions of VOC/O_2 molar ratio = 1/300 and SV = 30,000 mL/(g h).

Table 3
Catalytic performance of the chromia catalysts under the conditions of VOC concentration = 500 ppm, VOC/O_2 molar ratio = 1/300, and SV = 30,000 mL/(g h).

Catalyst	HCHO oxidation activity (°C)			Acetone oxidation activity (°C)			Methanol oxidation activity (°C)		
	$T_{10\%}$	$T_{50\%}$	$T_{90\%}$	$T_{10\%}$	$T_{50\%}$	$T_{90\%}$	$T_{10\%}$	$T_{50\%}$	$T_{90\%}$
bulk-Cr	90	152	–	76	142	–	80	164	–
meso-Cr-200	72	117	146	61	116	167	70	120	152
meso-Cr-300	50	100	122	40	90	142	52	105	136
meso-Cr-400	41	92	117	34	75	124	50	98	130
meso-Cr′-400	80	121	163	64	123	172	73	125	170
meso-Cr-500	61	108	134	52	108	158	59	112	147

there was no sign of partial oxidation of formaldehyde, acetone, and methanol over the chromia catalysts (CO_2 and H_2O being the only products) and the carbon balance of the reactions was ca. 99.5%.

According to the characterization results and catalytic activity data, we believe that the adsorbed oxygen species were mainly responsible for the catalytic combustion of the VOC molecules. Since the oxidation of the VOCs over the chromia catalysts took place at lower temperatures (<200 °C) where the adsorbed oxygen species were active, but lattice oxygen species became active at higher temperatures (>300 °C). The co-presence of multivalent chromium atoms was beneficial for the improvement in reducibility of the catalyst. During the reaction processes, chromium ions with various oxidation states involved in a redox process, in which the gas-phase oxygen was activated to adsorbed oxygen species that then reacted with the VOC molecules to produce CO_2 and H_2O, and the consumed adsorbed oxygen species were replenished with the gas-phase oxygen molecules. Similar conclusions have also been drawn by other authors [8,47].

The oxidation of VOCs over other catalysts has been investigated in the past. Tang et al. observed formaldehyde conversion of 10% and 100% over pure CeO_2 and MnO_x–CeO_2 (with a Mn/(Mn + Ce) molar ratio of 0.5), respectively, at 90 °C and SV = 30,000 mL/(g h) [47]. Gandía et al. prepared manganese oxides supported on Al- and Zr-pillared clays, and found that complete oxidation of acetone was achieved over these materials in the 337–387 °C range at SV = 34,000 h^{-1} [48]. After studying the catalytic activities of $La_{0.8}Sr_{0.2}MnO_{3+x}$ for the removal of a number of VOCs at 20,000 h^{-1}, Blasin-Aubé et al. [6] reported that propanal, acetone, and ethanol could be completely converted to CO_2 and H_2O at 350 °C. It is clear that the *meso*-Cr-400 catalyst was much superior to the MnO_x/Al (or Zr)-pillared clay [48] and $La_{0.8}Sr_{0.2}MnO_{3+x}$ catalysts [6] but slightly inferior to the MnO_x–CeO_2 catalyst [47] in catalytic performance.

Several researchers have investigated the kinetics related to the combustion of VOCs such as butyl acetate [49], propane [50], methanol [51], and methanol and formaldehyde [52], and it is generally believed that the reactions are first-order with respect to the VOC. Similarly, the oxidation of formaldehyde, acetone, and methanol under the reaction conditions adopted in the present study would follow a mechanism of first-order reaction toward the VOC. It has been reported that the oxidation of VOCs (e.g., benzene, toluene, and trichloroethylene) over transition-metal-based oxide catalysts was first-order and zero-order with respect to VOC and O_2, respectively [7,49,53]. In the present investigation, the O_2 amount (VOC/O_2 molar ratio = 1/300) was excessive, as compared to the theoretical O_2 amounts (VOC/O_2 molar ratio = 1/1–1/4) required for total oxidation of the VOCs. Considering the similarities in nature of the VOCs and catalysts as well as in reaction condition, it is reasonable to assume that the oxidation of formaldehyde, acetone or methanol over the mesoporous chromia catalysts was zero-order with respect to O_2.

Fig. 10 illustrates the Arrhenius plots of catalytic oxidation of formaldehyde, acetone, and methanol over *meso*-Cr-400. The apparent activation energy for the combustion of formaldehyde, acetone, and methanol over *meso*-Cr-400 was calculated to be 45.6, 49.7 and 50.8 kJ/mol, respectively. It is known that the apparent activation energies for formaldehyde, acetone, and methanol oxidation are highly dependent on the nature of the employed catalyst. For example, apparent activation energy was 33 kJ/mol over 10 wt% MnO_x/SiO_2 [54] and ca. 49 kJ/mol over 1 wt% Pt/TiO_2 [55] for acetone oxidation. It was 60.3 kJ/mol over Pt/γ-Al_2O_3 for methanol oxidation (in the range of 100–130 °C) [56]; 37.3 kJ/mol over 0.1 wt% Pt/fluorinated carbon [57] and 57.1 kJ/mol over 1 wt% Pt/TiO_2 [55] for formaldehyde oxidation. One can see that the apparent activation energies for the addressed reactions over the mesoporous chromia catalysts were close to those over the supported MnO_x or Pt catalysts.

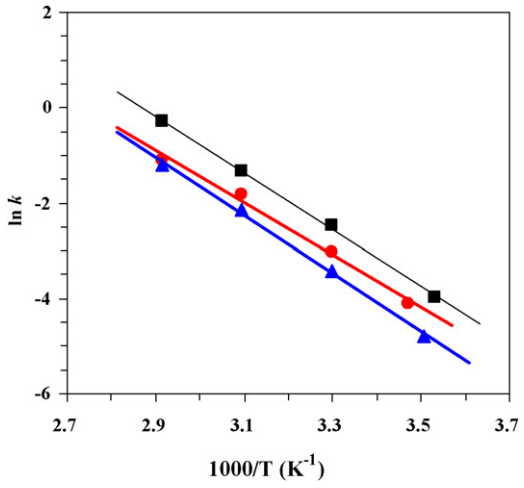

Fig. 10. Arrhenius plots for the oxidation of formaldehyde (●), acetone (■), and methanol (▲) over the *meso*-Cr-400 catalyst under the conditions of VOC concentration = 500 ppm, VOC/O_2 molar ratio = 1/300, and SV = 30,000 mL/(g h).

4. Conclusion

High-surface-area (69–124 m^2/g) rhombohedral chromia catalysts with 3D ordered mesoporous structures and polycrystalline pore walls were fabricated by means of an ultrasound-assisted KIT-6-templating strategy, using chromium nitrate as metal source and calcined in the 200–500 °C range. There was the co-presence of Cr^{3+}, Cr^{5+}, and Cr^{6+} ions in the mesoporous catalysts. The catalytic activities over the mesoporous chromia were much higher than that over the bulk counterpart. The *meso*-Cr-400 catalyst that showed the best reducibility performed the best, displaying $T_{90\%}$ = 117, 124, and 130 °C, respectively, for the complete oxidation of formaldehyde, acetone, and methanol at SV = 30,000 mL/(g h). The corresponding apparent activation energy was 45.6, 49.7, and 50.8 kJ/mol over the *meso*-Cr-400 catalyst. It is concluded that the ultrasound treatment during the nanocasting process facilitated the improvement in mesoporosity quality of the chromia materials and the excellent catalytic performance of *meso*-Cr-400 was associated with the low-temperature reducibility, 3D ordered mesoporous architecture, and high-surface area of *meso*-Cr-400.

Acknowledgements

The work described above was supported by the NSF of China (grant No. 20973017), the Creative Research Foundation of Beijing University of Technology (00500054R4003), the "863" Key Program of Ministry of Science and Technology of China (2009AA063201), the PHR200907105 of the Beijing Municipal Commission of Education, and the NSF of Beijing Municipality (Key Class B project of grant No. KZ200610005004).

References

[1] J.N. Armor, Appl. Catal. B 1 (1992) 221–256.
[2] D. Andreeva, R. Nedyalkova, L. Ilieva, M.V. Abrashev, Appl. Catal. B 52 (2004) 157–165.
[3] F. Kovanda, T. Rojka, J. Dobešová, V. Machovič, P. Bezdička, L. Obalová, K. Jirátová, T. Grygar, J. Solid State Chem. 179 (2006) 812–823.
[4] F. Wyrwalski, J.-F. Lamonier, S. Siffert, A. Aboukaïs, Appl. Catal. B 70 (2007) 393–399.
[5] D. Delimaris, T. Ioannides, Appl. Catal. B 84 (2008) 303–312.
[6] V. Blasin-Aubé, J. Belkouch, L. Monceaux, Appl. Catal. B 43 (2003) 175–186.
[7] M. Alifanti, M. Florea, V.I. Pârvulescu, Appl. Catal. B 70 (2007) 400–405.
[8] X.Z. Yang, Y.N. Shen, Z.F. Yuan, H.Y. Zhu, J. Mol. Catal. A 237 (2005) 224–231.
[9] X.F. Tang, X.M. Huang, J.J. Shao, J.L. Liu, Y.G. Li, Y.D. Xu, W.J. Shen, Chin. J. Catal. 27 (2006) 97–99.
[10] T. Chen, H.Y. Dou, X.L. Li, X.F. Tang, J.H. Li, J.M. Hao, Micropor. Mesopor. Mater. 122 (2009) 270–274.
[11] M.C. Álvarez-Galván, V.A. de la Peña O'Shen, J.L.G. Fierro, P.L. Arias, Catal. Commun. 4 (2003) 223–228.
[12] M. Baldi, E. Finocchio, F. Milella, G. Busca, Appl. Catal. B 16 (1998) 43–51.
[13] Y. Xi, C. Reed, Y.K. Lee, S.T. Oyama, J. Phys. Chem. B 109 (2005) 17587–17596.
[14] F. Jiao, A. Harrison, A.H. Hill, P.G. Bruce, Adv. Mater. 19 (2007) 4063–4066.
[15] C. Dickinson, W. Zhou, R.P. Hodgkins, Y. Shi, D. Zhao, H. He, Chem. Mater. 18 (2006) 3088–3095.
[16] F. Jiao, A. Harrison, J.-C. Jumas, A.V. Chadwick, W. Kockelmann, P.G. Bruce, J. Am. Chem. Soc. 128 (2006) 5468–5474.
[17] Y. Wang, C.M. Yang, W. Schmidt, B. Spliethoff, E. Bill, F. Schüth, Adv. Mater. 17 (2005) 53–56.
[18] R. Ryoo, S.H. Joo, S. Jun, J. Phys. Chem. B 103 (1999) 7743–7746.
[19] A.K. Sinha, K. Suzuki, Angew. Chem. Int. Ed. 44 (2005) 271–273.
[20] A.K. Sinha, K. Suzuki, Appl. Catal. B 70 (2007) 417–422.
[21] J.G. Deng, L. Zhang, H.X. Dai, C.T. Au, Appl. Catal. A 352 (2009) 43–49.
[22] J.R. Niu, J.G. Deng, W. Liu, L. Zhang, G.Z. Wang, H.X. Dai, H. He, X.H. Zi, Catal. Today 126 (2007) 420–429.
[23] J.G. Deng, Y. Zhang, H.X. Dai, L. Zhang, H. He, C.T. Au, Catal. Today 139 (2008) 82–87.
[24] J.G. Deng, L. Zhang, H.X. Dai, H. He, C.T. Au, J. Mol. Catal. A 299 (2009) 60–67.
[25] J.G. Deng, L. Zhang, H.X. Dai, H. He, C.T. Au, Catal. Lett. 123 (2008) 294–300.
[26] J.G. Deng, L. Zhang, H.X. Dai, C.T. Au, Catal. Lett. 130 (2009) 622–629.
[27] J.G. Deng, L. Zhang, H.X. Dai, H. He, C.T. Au, Ind. Eng. Chem. Res. 47 (2008) 8175–8183.
[28] Y.S. Xia, H.X. Dai, H.Y. Jiang, J.G. Deng, H. He, C.T. Au, Environ. Sci. Technol. 43 (2009) 8355–8360.
[29] F. Kleitz, S.H. Choi, R. Ryoo, Chem. Commun. (2003) 2136–2137.
[30] L. Li, Z.F. Yan, G.Q. Lu, Z.H. Zhu, J. Phys. Chem. B 110 (2006) 178–183.
[31] A. Małecki, R. Gajerski, S. Łabuś, B. Prochowska-Klisch, K.T. Wojciechowski, J. Therm. Anal. Calorim. 60 (2000) 17–23.
[32] K.K. Zhu, B. Yue, W.Z. Zhou, H.Y. He, Chem. Commun. (2003) 98–99.
[33] F. Jiao, P.G. Bruce, Adv. Mater. 19 (2007) 657–660.
[34] Y.G. Wang, X.H. Yuan, X.H. Liu, J.W. Ren, W.Y. Tong, Y.Q. Wang, G.Z. Lu, Solid State Sci. 10 (2008) 1117–1123.
[35] K. Jiao, B. Zhang, B. Yue, Y. Ren, S.X. Liu, S.R. Yan, C. Dickinson, W.Z. Zhou, H.Y. He, Chem. Commun. (2005) 5618–5620.
[36] F. Jiao, A.H. Hill, A. Berko, A.V. Chadwick, P.G. Brue, J. Am. Chem. Soc. 130 (2008) 5262–5266.
[37] A. Rumplecker, F. Kleitz, E.L. Salabas, F. Schüth, Chem. Mater. 19 (2007) 485–496.
[38] F. Cavani, M. Koutyrev, F. Trifirò, A. Bartolini, D. Ghisletti, R. Iezzi, A. Santucci, G. Del Piero, J. Catal. 158 (1996) 236–250.
[39] B.M. Weckhuysen, I.E. Wachs, R.A. Schoonheydt, Chem. Rev. 96 (1996) 3327–3349.
[40] H. Lu, D.H. Shen, C.L. Bao, Y.X. Wang, Phys. Status Solidi A 159 (1997) 425–437.
[41] J.R. Sohn, S.G. Ryu, Langmuir 9 (1993) 126–131.
[42] J.M. Rao, A. Sivaprasad, P.S. Rao, B. Narsaiah, S.N. Reddy, V. Vijayakumar, S.V. Manorama, K.L. Krishna, K. Srinivas, K.R. Krishnan, S. Badrinarayanan, J. Catal. 184 (1999) 105–111.
[43] H. Rotter, M.V. Landau, M. Carrera, D. Goldfarb, M. Herskowitz, Appl. Catal. B 47 (2004) 111–126.
[44] L.I. Ilicva, D.H. Andreeva, Thermochim. Acta 265 (1995) 223–231.
[45] L. Storaro, R. Ganzerla, M. Lenarda, R. Zanoni, A.J. López, P. Olivera-Pastor, E.R. Castellón, J. Mol. Catal. A 115 (1997) 329–338.
[46] B. Graybowska, J. Słoczyński, R. Grabowski, K. Wcisło, A. Kozłowska, J. Stoch, J. Zieliński, J. Catal. 178 (1998) 687–700.
[47] X.F. Tang, J.L. Chen, X.M. Huang, Y.D. Xu, W.J. Shen, Appl. Catal. B 81 (2008) 115–121.
[48] L.M. Gandía, M.A. Vicente, A. Gil, Appl. Catal. B 38 (2002) 295–307.
[49] C.T. Wong, A.Z. Abdullah, S. Bhatia, J. Hazard. Mater. 157 (2008) 480–489.
[50] T.F. Garett, E. Rincón, C.R. Apesteguía, Appl. Catal. B 48 (2004) 167–174.
[51] S. Yao, F.O. Yang, S. Shimumora, H. Sakurai, K. Tabata, E. Suzuki, Appl. Catal. A 198 (2000) 43–50.
[52] Y. Wang, K. Otsuka, J. Catal. 155 (1995) 256–267.
[53] K. Everaert, J. Baeyens, J. Hazard. Mater. B109 (2004) 113–139.
[54] C. Reed, Y.K. Lee, S.T. Oyama, J. Phys. Chem. B 110 (2006) 4207–4216.
[55] R. Dewil, K. Everaert, J. Baeyens, Catal. Commun. 6 (2005) 793–795.
[56] J. Pasel, B. Emonts, R. Peters, D. Stolten, Catal. Today 69 (2001) 193–200.
[57] K.T. Chuang, B. Zhou, S. Tong, Ind. Eng. Chem. Res. 33 (1994) 1680–1686.